Proc. Natl. Sci. Counc. ROC(A)
Vol. 23, No. 2, 1999. pp. 235-247

Soil Movements Around a Tunnel in Soft Soils

CHUNG-JUNG LEE, BING-RU WU, AND SHEAN-YAU CHIOU

Department of Civil Engineering
National Central University
Chungli, Taiwan, R.O.C.

(Received December 10, 1997; Accepted July 21, 1998)

ABSTRACT

Tunnelling in soft soils may cause ground movements and damage to adjacent buildings and overlying facilities. Ground movements around a tunnel before and after collapse have been investigated by conducting a series of tests with centrifuge tunnel models. This paper briefly describes the test procedures undertaken and summarizes a comparison of test results and field measurements relevant to the analysis of the extent of surface and subsurface settlement troughs. The observed overload factor at collapse was well bounded by the theoretical upper bound and lower bound solutions for tunnels with cover-to-diameter ratios of from 0.5 to 4. The proposed collapse mechanism derived from the theoretical upper bound solution is consistent with that observed from the velocity fields of the model tests. The magnitude and extent of settlement troughs at different elevations under different values of ground loss for tunnels embedded at different depths are provided as well. It is suggested that these simple relationships can be usefully adopted by engineers for designing protective measures in buildings when considering the likely settlement of structures or substructures above a tunnel.

Key Words: collapse mechanism, overload factor, surface settlement trough, subsurface settlement trough, tunnel

I. Introduction

The more urbanized a city becomes, the more urgent the need is for an underground rapid transit system. Shield tunnelling has become more and more widely used in subway construction in soft soils to reduce interference with surface traffic during construction in Taiwan. However, inward soil movement due to the stress released by tunnelling inevitably causes ground movement around a tunnel. If these movements become excessive, they can damage adjacent buildings and overlying facilities. The prediction of surface and subsurface settlement troughs and the assessment of tunnel stability are very important parts of the designer's task of ensuring safe construction and appropriate protective measures for buildings situated near a tunnel project. Several researchers have studied the patterns of a settlement trough and tunnel stability problems using three different approaches, i.e., empirical, numerical, and physical modelling approaches. These three approaches to solving these problems have their own advantages and limitations. In this study, a series of tests with centrifuge tunnel models was used to examine the ground movement around a tunnel in soft soils before and after collapse.

Peck (1969) first suggested that the shape of a transverse surface settlement trough over a tunnel might approximate closely a Normal Probability Curve from the field measurements as follows:

$$S(x) = S_{\max}\exp\left(-\frac{x^2}{2i^2}\right), \quad \textbf{(1)}$$

in which $S(x)$=the settlement at the offset distance, x from the tunnel centerline, and $S_{\max}$=the maximum surface settlement at the point above the tunnel centerline. The width parameter i is the distance from the centerline to the inflection point of the trough and may be employed as a measure of the shape and extent of the settlement trough. The distance from the centerline to the point of minimum curve radius is $\sqrt{3}i$. Two and one half times i is commonly used to represent the half width of the settlement trough, w. This shape is shown in Fig. 1.

Peck (1969) and Cording and Hansmire (1975) presented a normalized relationship of the width parameter, $2i/D$, versus the tunnel depth, z/D, for tunnels driven through different geological conditions. That is:

$$\frac{2i}{D} = \left(\frac{z}{D}\right)^{0.8}, \quad \textbf{(2)}$$

in which D is the diameter of the tunnel, and z is the

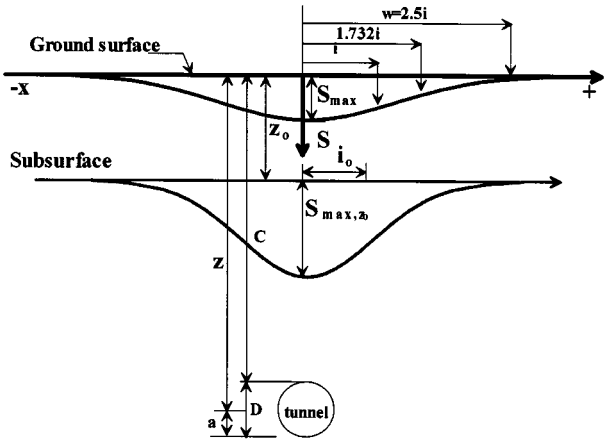

Fig. 1. Form of surface and subsurface settlement profiles.

centerline depth of the tunnel. Fujita (1982) statistically analyzed the maximum surface settlement caused by shield tunnelling based on 94 cases in Japan. He suggested a reasonable range of S_{max} for different types of shield machines driven through different soil conditions, with or without additional measures. Fang *et al*. (1994) combined Fujita's suggestion with Peck's experience and proposed an empirical method to estimate the magnitude and extent of the surface settlement trough. It was found that the predicted surface settlement troughs were consistent with the field measurements. The empirical method is frequently used in engineering practice; however, it has no theoretical justification. Moreover, critical information immediately preceding the collapse of a tunnel is not available because of the obvious danger. Therefore, it is not possible to understand the mechanism involved by means of observation alone.

Experiments using physical models have been carried out for many years in many research fields to discover and understand the behavior and the properties of physical systems. A mandatory condition upon which physical modelling is based is that the modelling system and the prototype system must obey the same physical laws. Furthermore, the modelling system must be constructed so as to embody all of the relevant features and parts of the prototype system. The conditions of similarity between the two systems must exist. When one reviews the similarity conditions which must be satisfied in a scaled model, it is obvious that the model behavior in situations where gravity effects are important can not properly replicate the full-scale prototype unless the model is tested under an increased body force field. In order that the gravity-induced stress is properly simulated, it is necessary to test a 1/*N*th scaled model in a gravity field *N* times stronger than the level experienced by the prototype situated in the earth's gravity field. The stable centrifugal force is the most economical and easiest way to produce a repeatable man-made gravity force field. In recent years, centrifuge models have proven to be useful for investigating the problems related to shield tunnelling because such a construction is entirely a gravity problem. A centrifuge tunnel can competently provide an opportunity to continuously observe the deformation and collapse of a tunnel in safety. There have been many research works related to centrifuge modelling of tunnels over the past decade (Chambon and Corte, 1994; Mair *et al*., 1984; Takemura *et al*., 1990). However, these researches did not directly compare test results with field measurements.

The construction operation for shield tunnelling consists of excavation of a tunnel face using miners and machinery protected within a shield. A permanent tunnel lining is erected within the tailskin as the shield advances. Grout is usually placed between the lining and surrounding soil. Because the process is very complicated, it is obviously impossible to duplicate all of the details of the tunnelling process within a small-scale centrifuge model. Approximations need to be made in the model so that key features in engineering practice can be easily investigated. In simulating the construction of a shield tunnel in soft soil, consideration must be given to ground loss caused by overcutting due to (1) the difference between the diameter of the tunnelling machines and that of the lining; (2) three dimensional soil movements ahead of the tunnel face; (3) alignment problems encountered when steering the shield by workmen lacking in experience; and (4) the effectiveness of tail void grouting. The net effect of these factors may be approximately incorporated into a two dimensional plane strain case in terms of annual voids. This volume can be represented using the crown deformation, S_c. However, the relationship between the void volume and maximum surface settlement has not been precisely evaluated in field case studies.

In this study, a plane strain model as shown in Fig. 2 was investigated as a good representation of tunnelling-induced ground movements. The tunnel model, 6 cm in diameter, was embedded at a depth with a specified cover-to-diameter ratio (*C*/*D*) and tested in a centrifugal gravity field of 100 g to model a prototype tunnel 6 m in diameter embedded at a depth with the same *C*/*D*, where *C* is the cover above the tunnel crown. A series of centrifuge model tests on tunnels with *C*/*D* ranging from 0.5 to 4.0 was carried out. In addition, limit analysis was conducted to find the upper bound and lower bound solutions for this simplified centrifuge model. This paper briefly describes the test series

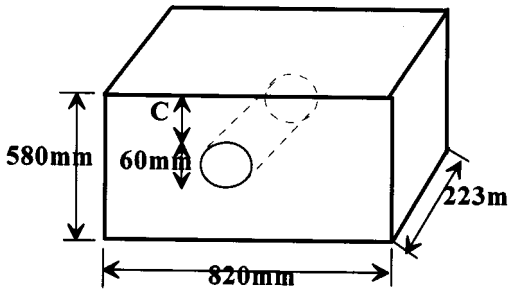

Fig. 2. The plane strain tunnel model.

undertaken and summarizes comparisons of the test results with field measurements directly relevant to analysis of the extent of surface and subsurface settlement troughs.

II. Test Equipment

1. NCU Geotechnical Centrifuge

This experimental work was undertaken at the geotechnical centrifuge in National Central University (NCU). This medium size centrifuge is housed in a circular underground enclosure 7 m in diameter by 3 m in height. The basic machine configuration and assembly have been described by Lee *et al*. (1997). The NCU geotechnical centrifuge, with a nominal radius of 3 m, is capable of accelerating a 1 ton model package to 100 g and a 0.55 ton package to 200 g. The room available for the payload in the swing basket has a depth of 100 cm, a width of 80 cm, a height of 80 cm, and a maximum height of 120 cm. The hydraulic rotary joint provides six hydraulic or pneumatic passages to the test package. An HP3852A data acquisition system mounted at the rotation center of the centrifuge in conjunction with an optic fiber rotary joint can log all of the data at a specified time interval and store it in a computer housed in the control room simultaneously. A closed circuit television provides in-flight monitoring.

2. Rectangular Consolidometer

The tested soil beds were consolidated in a rectangular consolidometer. The rectangular consolidometer as shown in Fig. 3 includes (1) a consolidometer box; (2) an extension piece; (3) a loading frame; and (4) a loading rigid plate with a bello-frame cylinder. The internal dimensions of the consolidometer box are length 820 mm, width 450 mm and height 480 mm. Two U-type liners and a thin plate spacer may be put into the consolidometer box to simultaneously prepare two cakes of soil beds having identical strength profiles.

3. Model Container

The geotechnical centrifuge model test is normally a simulation of the behavior of an infinite half space subjected to a localized perturbation. The model must be held within the container so that the container boundaries will replicate the behavior of the far field half-space. Since the extent of the settlement trough calculated using Eq. (2) for the prototype tunnel with a cover-to-diameter ratio equal to 4 was 49.96 m, the coverage of the settlement trough in the tunnel model was 49.9 cm in a centrifugal gravity field of 100 g. The internal dimensions of the container used in the study were length 820 mm, width 223 mm and height 580 mm, as shown in Fig. 4. Therefore, the length of the container was large enough to reduce the boundary effects. The container was manufactured using high strength Aluminum Alloy. The stiffness of the sidewall was strong enough to satisfy a plane strain condition in the model. For static testing, the lateral displacement of the container wall was set less than about 0.1% of the retained height of the soil to insure a minimal effect

Fig. 3. The rectangular consolidometer.

Table 1. Test Conditions and Mechanical Properties of Clay Beds

Test No.	tunnel diameter D, (cm)	cover-to-diameter (C/D)	undrained shear strength S_u, (kPa)	secant modulus E_{50}, (kPa)	initial tangent modulus E_i, (kPa)
Test2	6	2	41.3	2114	–
Test3	6	2	30.2	1370	–
Test4	6	1	37.0	1746	–
Test5	6	1	36.9	1317	2756
Test6	6	3	30	660	2920
Test7	6	3	30	1091	2847
Test8	6	1	37.9	1486	2684
Test9	6	2	35.8	1278	2367
Test10	6	4	32.2	1308	2510
Test11	6	0.5	31.0	–	–
Test12	6	0.5	35.1	1157	2039

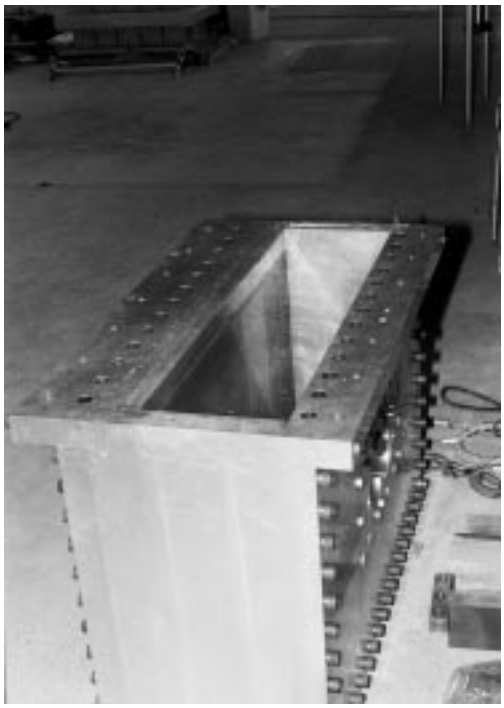

Fig. 4. The model container.

on the lateral earth pressure. One of sidewalls was made of transparent acrylic in order to permit viewing of the subsurface events. In addition, lubricating the walls with water-resistant grease before each test could considerably reduce the sidewall friction.

III. Test Material

The soil used in all of the model tests was taken from the NCU campus. The tested soil, with a plasticity index of 18, was classified into CL using the Unified Classification System. It was ground so as to pass through a #40 sieve and submerged in water for two days before preparation of the reconstituted soil beds. The method of preparation of the reconstituted soil beds is described in the following section. Extensive research has been carried out to obtain the parameters of the Cam clay model for this reconstituted sample. The value of the effective friction angle was 33 degrees (Lee *et al.*, 1997).

IV. Test Procedures

In this study, the test procedures were divided into four stages. The details of the procedures are as follows.

1. Preparation of Soil Beds

The tested soil was remolded at about twice its liquid limit in a mixer. Two U-type liners and a plate spacer were put into the consolidometer box, and then a drainage sand layer with a thickness of 5 cm was used to cover the bottom of the consolidometer box. The slurry was poured in four layers and subjected to a vacuum for two hours to remove any entrained air in each layer.

Upon completion of the consolidometer assemblage, the initial increment of consolidation pressure used was 10 kPa. After this first increment, the consolidation pressure was successively doubled until the required maximum consolidation pressure (225 kPa) was achieved. Consolidation was monitored by measuring the vertical displacement of the loading piston. It took one month to prepare two cakes of soil beds. The undrained shear strength profiles of the consolidated soil beds as listed in Table 1 are nearly the same as that of silty clay from the Taipei Basin. At the elevation of the tunnel center, i.e., 11 m to 15 m below

the surface in the prototype scale, the average undrained shear strength is about 30-45 kN/m^2 for the Taipei Silty clay in the Taipei Basin.

2. Reconsolidation of Soil Beds

Upon completion of consolidation, the loading frame, the loading rigid plate with a bello-frame cylinder and the extension piece were removed. The consolidometer box and the soil bed were exposed. After shaping the soil beds, one cake of soil bed together with its U-type liner was lifted up and put into the model container.

Five pore water pressure transducers (PPTs) were instrumented at the selected positions, and a row of nine linear variable differential transformers (LVDTs) was placed on the surface and along the model centerline, respectively. The test package was then lowered down onto the platform of the centrifuge. After mounting the package and adjusting the position of the counter-weight on the centrifuge arm, the centrifugal acceleration was increased to 100 g in 10 g increments. The pore water pressures and surface settlements were continuously measured during flight. The centrifuge was decelerated until the pore water pressures and settlements reached stable values.

3. Model Making

After the first acceleration, the package was taken out of the centrifuge. The LVDTs and the front acrylic wall of the container were removed. A tunnel 6 cm in diameter was carefully cut out and lined with a rubber bag of negligible stiffness and strength. Four deformation gauges, made of four thin sliced strain-gaged cantilevers, were put inside the rubber bag. The free end of each cantilever was bonded to its position on the inner surface of the bag. Therefore, the deformations of the crown, invert, and two sidewalls of the tunnel could be measured during the subsequent collapse tests. A row of marked spaghetti was implanted along the center of the model. Spaghetti absorbs water from the surrounding soil and will displace in the same manner as the soil. This is a good indicator for depicting soil movement in a model. After these operations, the front acrylic wall and LVDTs were put back into their positions. The package was placed back onto the platform again, and all transducers were connected to an HP3852A. The entire electrical setup for the test package is shown in Fig. 5. An air pressure line was then connected to the rubber bag. The applied air pressure p_i was equivalent to the excess air or slurry pressure in a tunnel heading during construction. The package was ready

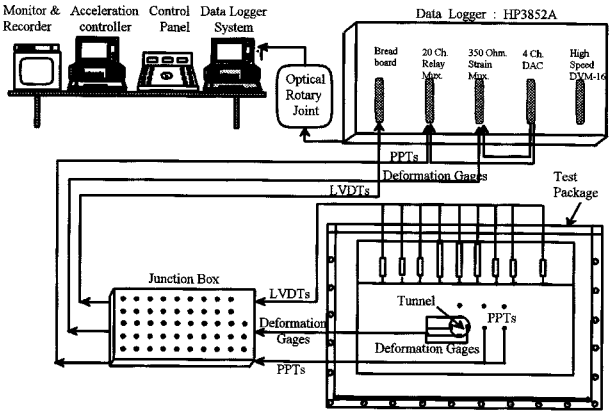

Fig. 5. Electrical setup of the test package.

to perform the tunnel collapse test in the second acceleration.

4. Tunnel Collapse Test

The centrifuge acceleration was increased to 100 g in 5 g increments. At each increment, the air pressure in the rubber bag was cautiously regulated so that it would serve as a support pressure for the tunnel and no surface settlement would occur. The model was allowed to rotate at 100 g for about 10 minutes. Then, the tunnel collapse test was performed by gradually reducing the air pressure to zero at increments of 10 kPa each 30 seconds. The pore water pressures, deformations at the crown, invert, and two sidewalls and the surface settlements were continuously recorded. After centrifuge flying stopped, the tension cracks on the surface of the model were evident, and the distances between the major tension cracks appearing on the two sides of the tunnel was measured. The soil bed was immediately excavated to expose the spaghetti. The deformation pattern of the soil around the tunnel was plotted. At the same time, six undisturbed samples at selected depths were taken to obtain the profile of the undrained shear strength and water contents along each depth.

In total, eleven tests were conducted. Table 1 lists the mechanical properties of the tested clay beds and test conditions. The typical strength profile was between 30 kPa and 45 kPa.

V. Elastic-Plastic Analysis Around a Tunnel

1. Stresses Around a Tunnel

The analysis assumes that a circular tunnel of initial radius a is embedded in an infinite space. The

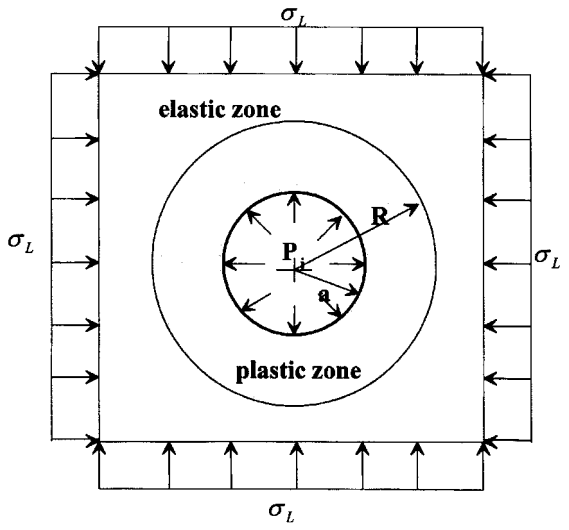

Fig. 6. Analytical mode of a tunnel.

length of the tunnel is such that the problem can be treated as a two dimensional and axial symmetrical case. Figure 6 shows the analytical model. The horizontal and vertical stresses are assumed to be equal and have a magnitude σ_L:

$$\sigma_L=\sigma_{vo}+\sigma_s, \tag{3}$$

where σ_{vo}=the vertical overburden pressure at the tunnel axis and σ_s=the surcharge on the surface. The installed support is assumed to exert a uniform support pressure, p_i, on the tunnel wall. The soil properties are assumed to be linear-elastic before failure and to be perfect plastic after the principal stress difference reaches the undrained shear strength, S_u. The failure criterion is defined as:

$$\sigma_1-\sigma_3=2S_u. \tag{4}$$

Here, σ_1 and σ_3 are the major and minor principal stresses, respectively.

For the case of cylindrical symmetry, the differential equation for equilibrium in the radial direction (Hearn, 1985) is:

$$\frac{d\sigma_r}{dr}+\frac{(\sigma_r-\sigma_\theta)}{r}=0, \tag{5}$$

in which σ_r=the radial stress and σ_θ=the tangential stress. Assume that the radius of the boundary of the elastic and plastic zone is R, and that the radial stress on the boundary is σ_{rp}. Then, satisfying Eq. (5) for linear-elastic behavior and the boundary conditions ($\sigma_r=\sigma_{rp}$ at $r=R$; $\sigma_r=\sigma_L$ at $r=\infty$) leads to the following equations for the stresses in the elastic zone:

$$\sigma_r=\sigma_L-(\sigma_L-\sigma_{rp})(\frac{R}{r})^2 \quad (r>R) \tag{6a}$$

$$\sigma_\theta=\sigma_L+(\sigma_L-\sigma_{rp})(\frac{R}{r})^2 \quad (r>R). \tag{6b}$$

In contrast to the elastic zone, the annular region ($a\le r\le R$) is in the plastic zone. Integration of Eq. (5) and substitution of the boundary conditions $\sigma_r=p_i$ at $r=a$ leads to the radial stress in the plastic zone:

$$\sigma_r=p_i+2S_u\ln(\frac{r}{a}). \tag{7}$$

2. Limit Analysis for Stability Solution

Stability problems were obtained using the limit theorems of plasticity. According to the theory of plasticity, the collapse load for a particular configuration of loading on a perfectly plastic body is unique. The lower bound theorem states that if any stress field can be found which supports the loads and is everywhere in equilibrium without yield being exceeded, then the loads are lower than (or equal to) those for collapse. The upper bound theorem states that if a work calculation is performed for a kinematically admissible collapse mechanism, then the loads thus deduced will be higher than (or equal to) those for collapse. Since the support pressure resists the collapse of the soil into the tunnel, it is a negative load in the sense discussed above. The lower bound theorem will furnish a safe estimate for the support pressure required to maintain tunnel stability whereas the upper bound theorem will provide an unsafe estimate.

A. Lower Bound of Support Pressure

The annular plastic region around a tunnel embedded at a depth of $C+D/2$ may transmit upward to the surface as a result of a decrease in the support pressure. After the boundary of the annual plastic zone reaches the surface, all of the soil mass above the tunnel will be continuously displaced. The tunnel will be on the verge of collapse, and the surface settlement will increase rapidly. Therefore, this support pressure, p_L, may be reasonably defined as the lower bound of the support pressure. Hence, substituting $r=C+D/2$, $a=D/2$, and $\sigma_r=\sigma_L$ into Eq. (7), p_L is given as:

$$p_L=\sigma_L-2S_u\ln(\frac{2C}{D}+1). \tag{8}$$

B. Upper Bound of Support Pressure

The centrifuge tunnel model test can bring a model to the state of collapse at the same stress level as a

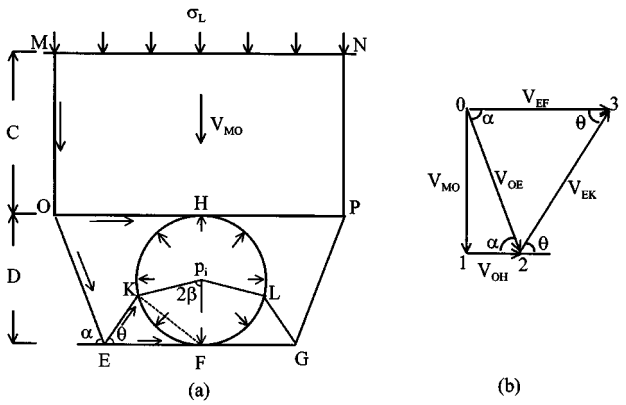

Fig. 7. Upper bound failure mechanism. (a) The sliding wedges. (b) The associated velocity diagram.

prototype. Hence, the mechanism for plastic collapse could be determined by referring to the observed velocity field of the marked spaghetti in this study. This collapse mechanism consists of five rigid wedges with three variables, α, β, and θ, as shown in Fig. 7(a). The associated velocity diagram is also shown in Fig. 7(b). Since this mechanism is symmetrical about the axis of the tunnel, it is only necessary to consider the movement on the left-hand side of Fig. 7(a). Wedge MNOP moves vertically downward along Line MO and Line NP as a rigid body. Its vertical downward velocity, V_{MO}, is taken to be one unit. The directions of velocity for Wedge HOEK relative to Wedge MNOP and relative to the zone which remains stationary are the same as the directions of the corresponding interfaces, i.e., Line OH and Line OE. However, Wedge HOEK in contact with Wedge MNOP must have the same vertical component of velocity as Wedge MNOP. The magnitudes of the velocity V_{OE} and the relative velocity V_{OH} are, therefore, determined uniquely. Similarly, the velocity V_{EF} and the relative velocity V_{EK} are determined as well. Using the notation ℓ_{OH} for the length of the interface OH, etc., the following work equation for the mechanism in the undrained condition is given as:

$$(\sigma_L - p_i)\ell_{OH} = S_u(C\times V_{MO} + \ell_{OH}\times V_{OH} + \ell_{OE}\times V_{OE} + \ell_{EK}\times V_{EK} + \ell_{EF}\times V_{EF}). \quad \textbf{(9)}$$

Expressing all of the velocities and lengths in terms of V_{MO}, α, β, θ, C, and D and then placing them into Eq. (9) give:

$$P_u = \sigma_L - S_u[\frac{C}{D} + \frac{1}{\sin^2\alpha} + \frac{\sin\beta\sin(\beta+\theta)}{\sin\theta\tan\alpha} + \frac{1}{\tan^2\alpha} + \frac{\sin^2\beta}{\sin^2\theta} + \frac{\sin\beta\sin(\beta+\theta)\sin(\alpha+\theta)}{\sin^2\theta\sin\alpha}]$$
$$/\,[\frac{\sin\beta\sin(\beta+\theta)}{\sin\theta} + \frac{1}{\tan\alpha}]. \quad \textbf{(10)}$$

Table 2. Solutions of Lower and Upper Bounds for Collapse Mechanisms

C/D	0.5	1.0	2.0	3.0	4.0
α	65°	61°	55°	51°	48°
β	33°	37°	43°	47°	50°
θ	84°	76°	67°	60°	55°
$(OF)_U$	2.87	3.35	4.15	4.82	5.41
$(OF)_L$	1.39	2.20	3.20	3.91	4.42

There are three independent variables in Eq. (10). The upper bound support pressure can be calculated by varying the combination of values of α, β, and θ for the tunnel with a cover-to-diameter ratio.

Construction engineers are concerned very much with ground movement during tunnelling. The collapse tests in this study were performed by gradually reducing the support pressure, p_i, so that the overload factor is defined as:

$$OF=(\sigma_{vo}-p_i)/S_u. \quad \textbf{(11)}$$

The factor is a good indicator for describing the collapse process in the tests. Table 2 lists the theoretical solutions for α, β, θ, and $(OF)_U$, calculated from Eq. (10), and $(OF)_L$, calculated from Eq. (8). This table shows that α and θ decrease with an increase of the cover-to-diameter ratio; however, β, $(OF)_U$, and $(OF)_L$ increase with an increase of the cover-to-diameter ratio. These facts prove that the coverage of a large settlement zone increases with the increase of the embedded depth of a tunnel even though a deeper tunnel has better stability. Using the upper bound and lower bound theorems, the support pressure at collapse p_c must be bounded from above and below.

VI. Test Results and Discussion

1. Tunnel Stability

Figure 8 is a plot of the surface settlements at different positions and crown settlements against OF for the tunnel with C/D equal to 3. The LVDT array used is also displayed below. The maximum surface settlement occurred at the position above the crown, and both the crown settlements, S_c, and the surface settlements, $S(x)$, increased slowly until the value of

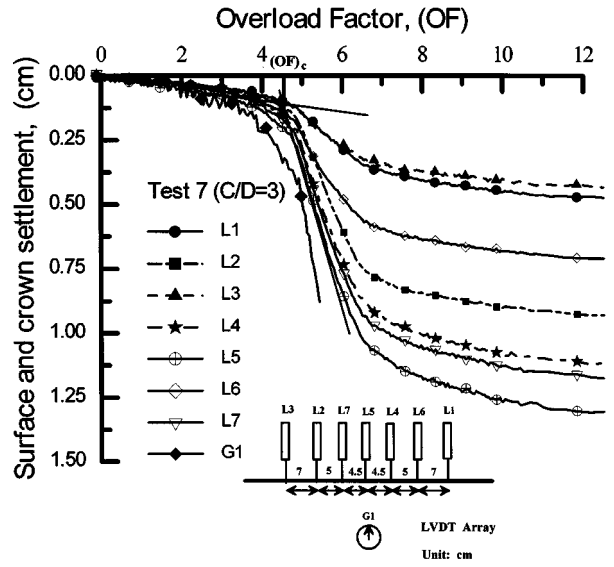

Fig. 8. Relationship between the surface settlement and overload factor along the transverse section.

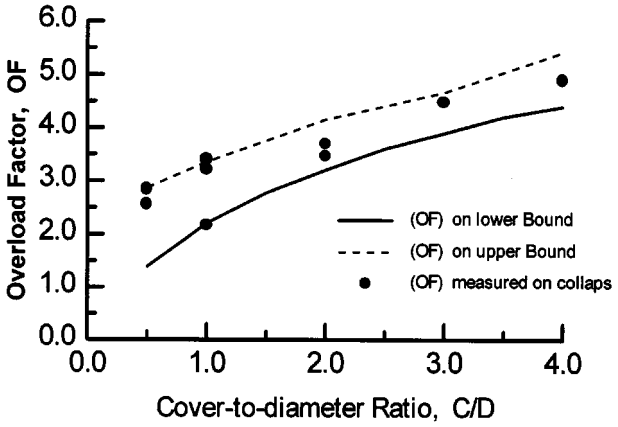

Fig. 9. Relationship between the cover-to-diameter ratio and the overload factor on the upper and lower bounds.

OF reached $(OF)_c$, as shown in Fig. 8. The following procedures were used to determine the overload factor at collapse, $(OF)_c$. The straight-line portions of first and second parts of the $S(x)$~OF curve measured at the centerline were extended to intersect at the point shown in Fig. 8. The ordinate of this point is regarded as $(OF)_c$. Then, the support pressure at collapse, p_c, could be calculated from the definition of $(OF)_c$. The lines shown in Fig. 9 are the theoretical lower and upper bound solutions (Eqs. (8) and (10)). The measured $(OF)_c$ is bounded well by the calculated lower and upper bound solutions.

The velocity field observed from the marked spaghetti after excavation together with the calculated collapse mechanism is shown in Fig. 10 for the model tunnel with C/D equal to 2. The soil mass above the tunnel moved almost vertically downward. Large deformations occurred only inside the zones bounded by the collapse mechanism. The directions of movement agreed considerably well with those in the mechanism. This implies that the collapse mechanism used here is appropriate, and that the calculated $(OF)_U$ was close to the actual value.

2. Width of Surface Settlement Trough

For a tunnel in soft soil requiring support to remain stable, the concept of a load factor may be useful from the engineering point of view. The load factor, which is the reciprocal of a factor of safety against collapse, can be defined as:

$$LF = \frac{\sigma_{vo} - p_i}{\sigma_{vo} - p_c}. \qquad \textbf{(12)}$$

Tunnels are often excavated under city streets or other places where settlement caused by tunnelling can have adverse effects. Hence, estimation of the trough width is important for designers and excavators. On the basis of the measured surface settlement, $S(x)$, the width parameter i can be determined by regression analysis with Eq. (1). The surface settlement profiles at different support pressures can be expressed by Eq. (1) using a set of parameters, S_{max}/D and i. They are plotted in Fig. 11 for the model tunnel with C/D equal to 3. These curves compare fairly well with the results measured using the LVDTs on the surface. All of the test results confirmed that the measured surface settlement trough could closely approximate a Normal Probability Curve.

The magnitude of i for a tunnel depends upon the embedded depth and the strength of the soil containing

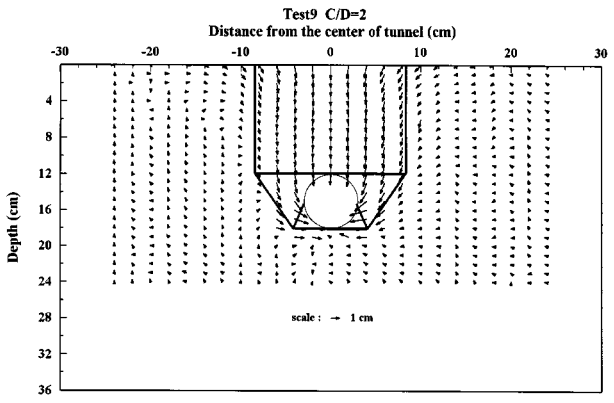

Fig. 10. Comparison of the observed velocity field and the calculated collapse mechanism.

Table 3. Observed and Analytical Parameters of Settlement Troughs

Test No:	C/D	(OF) at collapse	$\frac{S_{max}}{D}$ [a] at collapse	$\frac{i}{D}$ [b]	$\frac{\sqrt{3}i}{D}$	$\frac{w}{D}$ [c]	$\frac{B}{D}$ [d]	$\frac{TCD}{D}$ [e]
Test3	2	3.77	–	–	–	–	1.57	1.83-2.67
Test5	1	3.4	0.0483	0.96	1.67	2.72	1.3	1.67-2.17
Test6	3	4.86	0.0232	1.42	2.45	4.52	1.82	2.33-3.17
Test7	3	4.49	0.0237	1.53	2.65	4.82	1.82	2.5-3.5
Test8	1	3.22	0.0428	0.92	1.58	3.25	1.3	1.67-2.17
Test9	2	3.46	0.0342	1.25	2.17	4.25	1.57	2.17-3.0
Test10	4	5.0	0.0225	1.9	3.28	5.57	2.07	2.83-3.33
Test11	0.5	2.83	0.066	0.87	1.51	2.18	1.14	1.42-1.83
Test12	0.5	2.56	0.094	0.90	1.56	2.25	1.14	1.16-1.67

[a] S_{max} : Maximum surface settlement.
[b] i : Width parameter.
[c] w : Half width of the settlement trough.
[d] B : Half width of Wedge MNOP.
[e] TCD : Distance from the centerline of tunnel to the observed major tension cracks.

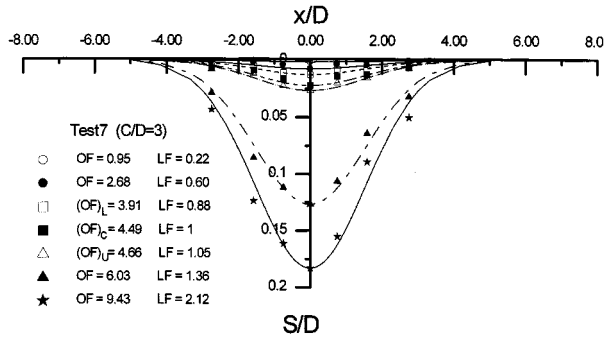

Fig. 11. Surface settlement troughs at different levels of load factors.

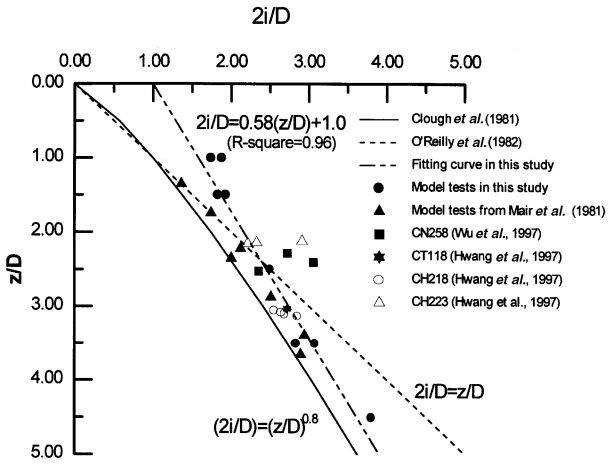

Fig. 12. Variation of the width of the surface settlement trough with the burial depth.

the tunnel. The relationship between $2i/D$ and z/D obtained from the results of the model tests in the study is determined as follows:

$$(\frac{2i}{D}) = 0.58 \times (\frac{z}{D}) + 1.0 \,. \qquad \textbf{(13)}$$

In order to examine Eq. (13) more closely, two different relationships of $2i/D$ and z/D proposed by Clough and Schmidt (1981) and O'Reilly and New (1982) are shown in Fig. 12. The centrifuge model test results from Mair *et al.* (1981) and the measured field data on Contracts CN-258 (Wu *et al.*, 1997), CH218 (Hwang *et al.*, 1995), CT118 and CH223 (Hwang *et al.*, 1997) are also plotted herein for comparison. These projects involved case histories of tunnelling in the Taipei basin. This figure shows that the relationship proposed by Clough and Schmidt (1981) underestimates the trough width while the relationship proposed by O'Reilly and New (1982) overestimates the trough width for deeper tunnels.

Table 3 is a list of the observed and analytical parameters of settlement troughs. Both S_{max} and i in Table 3 were measured at collapse. The distance from the tunnel centerline to the observed major tension cracks on the surface, TCD, and the half width of Wedge MNOP, B, as shown in Fig. 7(a), are also given. All of the parameters have been normalized with D to allow easy reference to the different tunnel sizes. The magnitude of i was nearly equal to the value of B, so that larger vertical displacements occurred in the zone within the two inflection points of the settlement trough. In the zone outside the settlement trough, however, no obvious settling was observed. Within these two zones, there was a transition zone. The quantity $\sqrt{3}i$ is the distance from the centerline to the point of maximum curvature of the settlement trough (Fig. 1). Here,

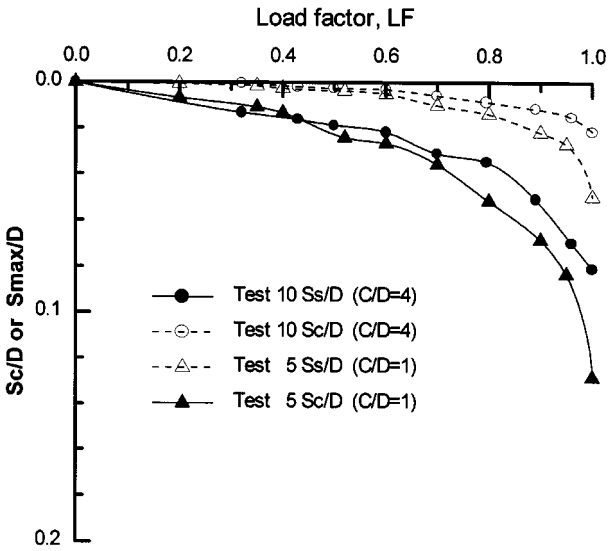

Fig. 13. Load factor against crown settlement and maximum surface settlement at different cover-to-diameter ratios.

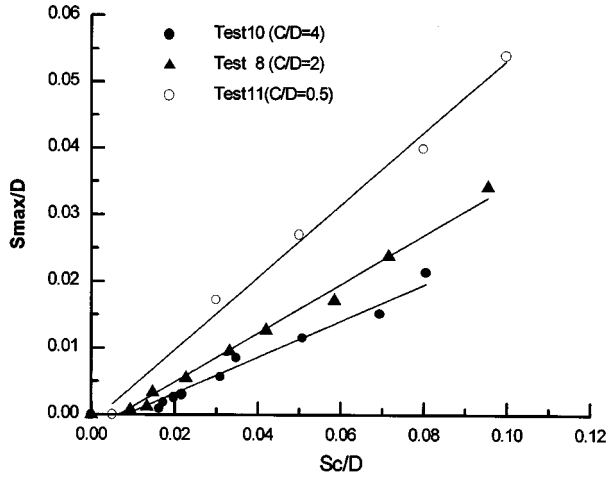

Fig. 14. Variation of maximum surface settlements with crown settlement.

$i<\sqrt{3}i<w$. Most of surface tension cracks appeared in the zone between the offset distance $\sqrt{3}i$ aud 2. 5i from the tunnel centerline.

3. Crown Settlement and Maximum Surface Settlement

The crown settlement, S_c, measured in the model tests can simulate the clearance between the cutting surface and the lining during tunnelling. The closure of the clearance was the primary cause of ground movement. Figure 13 shows the variation of the crown settlement and the maximum surface settlement as the support pressure was reduced and the load factor correspondingly increased. Both the crown and surface settlement were very small for load factors below 0.5, corresponding to a safety factor of 2.0. However, both types of settlement increased rapidly as the support pressure was further reduced. The magnitude of the crown settlement was larger than that of the maximum surface settlement. Figure 14 shows the variation of the maximum surface settlement in conjunction with the crown settlement as the support pressure was reduced. It is very interesting the ratios of S_{max} and S_c remained constant before a tunnel collapse. The magnitude of S_{max}/S_c for a tunnel depends upon the cover-to-diameter ratio, surface surcharge loading, and any compression or dilation in the soil around the tunnel. However, it may reasonable to assume that no volume change is involved in short-term settlement for a tunnel in soft clay, such as tunnelling in Taipei silty clay. Figure 15 shows a plot of the measured settlement ratio, S_{max}/S_c, versus the depth-to-diameter ratio, z/D, in the model test. The more shallow the tunnel, the greater the maximum surface settlement. These data points fit well with the line presented below:

$$\frac{S_{max}}{S_c} = 0.62\left(\frac{z}{D}\right)^{-0.58}. \qquad \textbf{(14)}$$

The magnitude of S_c is largely dependent on many factors, such as the volume of tail voids, the method of construction, workmanship factors, the presence or lack of back grouting, and grouting time. However, crown settlement may not be as easily measured in actual engineering practice as in model tests. Designers often use the percentage of ground loss, V_t, in place of S_c. The magnitude of S_c before tunnel collapse is relatively small compared with the tunnel diameter;

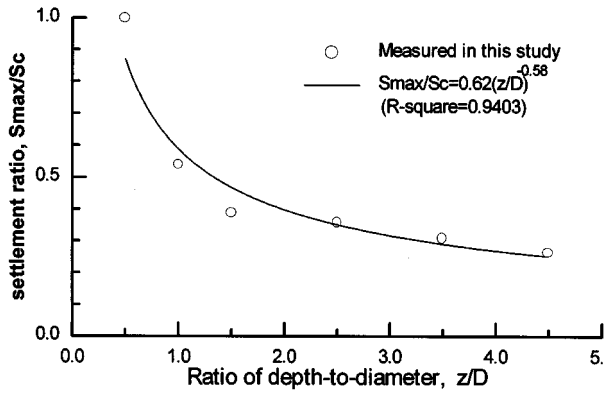

Fig. 15. Variation of settlement ratios with depth-to-diameter ratios.

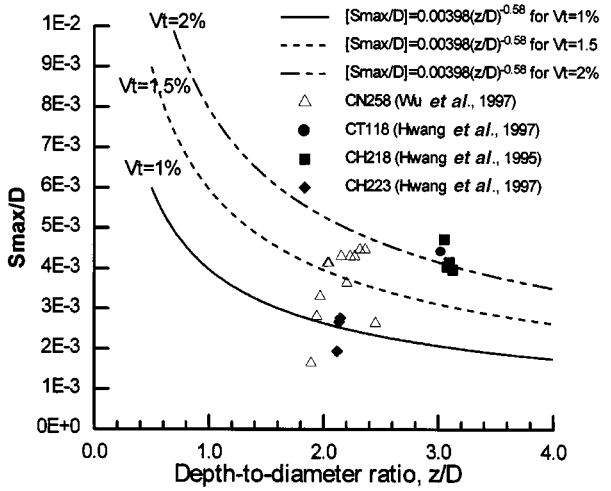

Fig. 16. Comparison of S_{max}/D predicted on the basis of model tests and from field measurements.

therefore, V_t can be written as:

$$V_t(\%) = \frac{4DS_{ave} - S_{ave}^2}{D^2} \times 100 \simeq \frac{400S_{ave}}{D} = \frac{156S_c}{D} . \quad \textbf{(15)}$$

Here, S_{ave} is defined as the average tunnel deformation measured at the crown, invert, and two sidewalls, and it is equal to $0.39S_c$ in the model tests. Therefore, substituting Eq. (15) into Eq. (14) gives

$$(\frac{S_{max}}{D}) = 0.00398(\frac{z}{D})^{-0.58} V_t(\%) . \quad \textbf{(16)}$$

Two lines derived from Eq. (16) for the cases of V_t(%) equal to 1% and 2% together with the measured maximum surface settlements corresponding to embedded depths from Contracts CN-258, CT118, CH218, and CH223 are plotted in Fig. 16. Here, S_{max} is the maximum surface settlement measured at an elapse time of 10 days after the passing of the shield as suggested by Hwang *et al*. (1995). The percentages of ground loss fall in the range of 1% to 2% for most of the measured points, as shown in Fig. 16. Moreover, the percentages of ground loss directly evaluated based on the volume of the measured settlement troughs in these projects range from 1% to 2% as well. Hence, the results confirm that Eq. (16) may be used to predict the maximum surface settlement for tunnelling projects in the Taipei Basin.

The magnitude of V_t , in general, can be evaluated prior to tunnel construction in the preliminary design stage; therefore, Eq. (16) together with Eq. (13) can be used to predict the surface settlement trough if V_t has been determined in advance.

4. Subsurface Settlement Profiles Above a Tunnel

Designers assessing the effects of tunnelling on structures relatively close to the tunnel crown need to know how subsurface settlement profiles develop and how these relate to surface settlement profiles. The effects on structures depend upon both the magnitude of settlement and the width of the subsurface settlement profile. In contrast to the surface settlement trough, few field measurements of subsurface settlement profiles are available to provide a relationship for performing such an assessment. It is often assumed that the subsurface settlement profile which develops at any depth may be approximated to a Normal Probability Curve in the same manner as can be a surface settlement trough. Figure 1 shows that a wider surface settlement trough with smaller settlement develops for a tunnel embedded at depth z below ground level. At a deeper level, at a distance $(z–z_o)$ above the tunnel axis, however, a narrower subsurface settlement trough with larger settlement develops. Hence, Eqs. (13) and (16) are applicable for predicting subsurface troughs if $z–z_o$ is substituted for z. They can be rewritten as:

$$(\frac{i_o}{z}) = 0.29 \times (1 - \frac{z_o}{z}) + \frac{D}{2z} \quad \textbf{(17)}$$

$$(\frac{S_{max,z_0}}{D}) = 0.00398(\frac{z - z_o}{D})^{-0.58} V_t(\%) , \quad \textbf{(18)}$$

in which i_o and S_{max,z_o} are the width parameter of a subsurface settlement trough and the maximum subsurface settlement at a distance $(z–z_o)$ above the tunnel axis, respectively.

The lines derived from Eq. (17) for tunnels embedded at different depth-to-diameter ratios (i.e., z/D from 1.5 to 7) are parallel to each other as shown in Fig. 17. The values of i_o obtained from the field measurements and the centrifuge model data (Mair *et al.*, 1993) at different distances, $(z–z_o)$, above the tunnel axis are also plotted in Fig. 17. The tunnel depths shown in Fig. 17 range from 20 m to 41 m, and the tunnel diameters are in the range of 3.786 m to 6.02 m. The relationship proposed by Mair *et al*. (1993) was

$$\frac{i_o}{z} = 0.175 + 0.325(1 - \frac{z_o}{z}) . \quad \textbf{(19)}$$

In this equation, the thick dotted line as shown in Fig. 17 does not take the burial depth into account; therefore, the width of the subsurface settlement profile will be significantly overestimated for the deeper tunnel. For a shallower tunnel, on the contrary, the width will

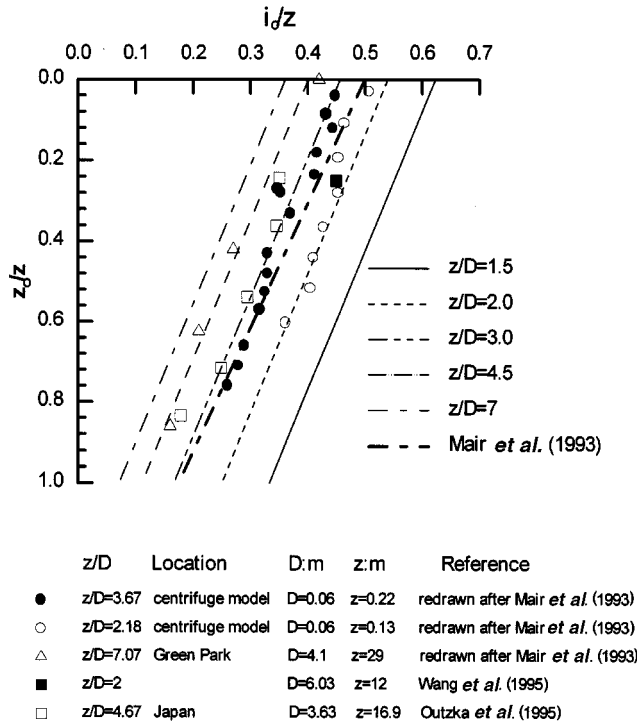

Fig. 17. Variation of the width parameter of a surface settlement trough with the depth for tunnels.

be underestimated. After examining Fig. 17 closely, the proposed relationship in the study is in reasonable agreement with the field measurements.

Substituting V_t=1% and 2% into Eq. (18) leads to the two lines shown in Fig. 18. These lines represent the possible range for V_t in engineering practice. The measured $S_{\max,z_o}$ at different levels of $(z-z_o)$ for six projects are plotted in Fig. 18 for comparison. Comparison of the measured subsurface settlements over a tunnel centerline and the predicted values from Eq. (18) shows reasonable agreement.

VII. Conclusions

Ground movements around a tunnel before and after collapse were carefully investigated by conducting a series of centrifuge model tests. A better understanding of ground movements has been obtained. The tested soil beds had nearly the same strength profiles as that in the Taipei Basin. Therefore, the results obtained from the model tests can be applied to actual engineering practice.

The proposed collapse mechanism derived from the theoretical upper bound solution in the limit analysis is consistent with the observed velocity fields in the model tests. The upper bound and lower bound solutions were derived for tunnels with different cover-to-diameter ratios. The observed overload factor at collapse is well bounded by the theoretical upper bound and lower bound solutions. The failure mechanism has never been obtained before from field measurements.

The immediate ground deformation around a tunnel is closely related to the load factor. Both the crown and the surface settlement increase dramatically at load factors over 0.5. This can serve as a guideline for excavators to provide the minimum support pressure in a tunnel in order to prevent the occurrence of greater ground movement.

The relationships between both i and $S_{\max}$ and z for different values of V_t have been proposed for the analysis of the surface settlement trough. In addition, the relationships between both i_o and $S_{\max,z_o}$ and $(z-z_o)$ for different values of V_t have also been provided for the analysis of the subsurface settlement trough. Comparison of field measurements and centrifuge model test results on both the surface and subsurface settlement troughs reveals a generally consistent pattern of settlement behavior. The advantage of the proposed relationship is simple and easy to use. It is suggested that these relationships can be adopted by engineers in designing protective measures of buildings when

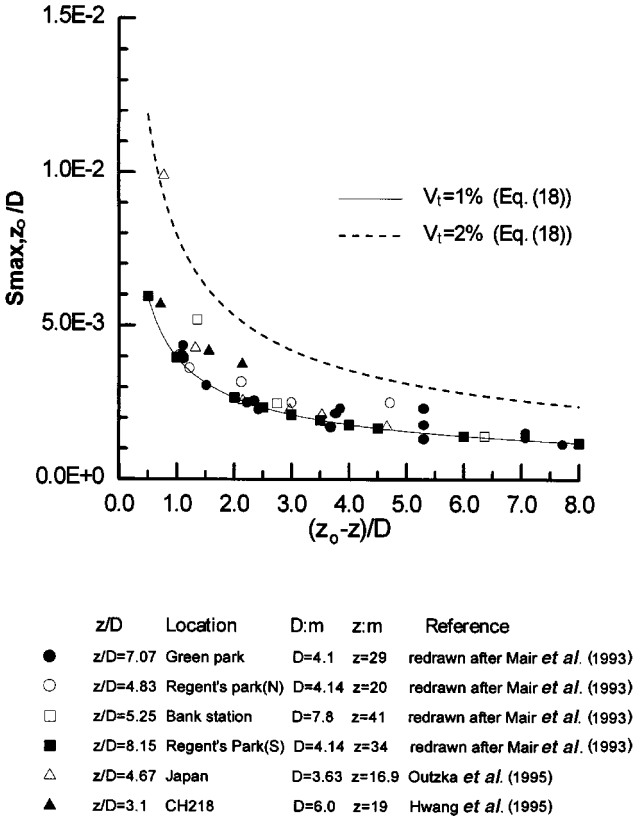

Fig. 18. Relationship between the subsurface settlement and the distance above the tunnel centerline.

considering the likely settlement of structures or sub-structures above tunnels.

Acknowledgment

Financial support provided by the National Science Council of the Republic of China under the Grants NSC 85-2732-E-008-007 and NSC 85-2611-E-008-003 is gratefully acknowledged.

References

Chambon, P. and J. F. Corte (1994) Shallow tunnels in cohesionless soil: stability of tunnel face. *J. Geotech. Eng.*, ASCE, **20**(GT7), 1148-1165.

Clough, G. W. and B. Schmidt (1981) Design and performance of excavations and tunnels in soft clay. In: *Soft Clay Engineering*, Chapter 8, pp. 569-634. Elsevier Scientific Publishing Company, Amsterdam, The Netherlands.

Cording, E. J. and W. H. Hansmire (1975) Displacement around soft ground tunnels. *Proceedings of the 6th Pan-American Conference on Soil Mechanics and Foundation Engineering*, pp. 571-633. Buenos Aires, Argentina.

Fang, Y. S., J. S. Lin, and C. S. Su (1994) An estimation of ground settlement due to shield tunnelling by the Peck-Fujita method. *Canadian Geotechnical Journal*, **31**, 431-443.

Fujita, K. (1982) Prediction of surface settlements caused by shield tunnelling. *Proceedings of the International Conference on Soil Mechanics*, Vol. 1, pp. 239-246. Mexico City, Mexico.

Hearn, E. J. (1985) *Mechanics of Materials*, 2nd Ed., pp. 667-672. Pergamon Press, New York, NY, U.S.A.

Hwang, R. N., C. B. Fan, and G. R. Yang (1995) Consolidation settlements due to tunnelling. *Proceedings of the South East Asian Symposium on Tunnelling and Underground Space Development*, pp. 79-86. Bangkok, Thailand.

Hwang, R. N., Y. S. Huang, T. L. Huang, and P. F. Yang (1997) Settlement troughs over tunnels. *Symposium on Construction and Underpinning for Rapid Transit System*, pp. 37-48. Sino-Geotechics Development and Research Foundations, Kaushung, Taiwan, R.O.C.

Lee, C. J., B. W. Wu, and C. S. Lin (1997) Calibration of undrained shear strength for clay beds in centrifuge modelling. *Proceedings of the Second International Symposium on Structures and Foundations in Civil Engineering*, pp. 208-213. Hong Kong.

Mair, R. J., M. J. Gunn, and M. P. O'Reilly (1981) Ground movement around shallow tunnels in soft clay. *Proceedings of the 10th International Conference on Soil Mechanics and Foundation Engineering*, pp. 323-328. Rio de Janeiro, Brazil.

Mair, R. J., R. Phillips, and A. N. Schofield (1984) Application of centrifuge modeling to the design of tunnels and excavation in soft clay. *Proceedings of the Symposium on the Application of Centrifuge Modelling to Geotechnical Design*, pp. 356-379. Manchester, U.K.

Mair, R. J., R. N. Taylor, and A. Bracegirdie (1993) Subsurface settlement profiles above tunnels in clays. *Geotechnique*, **43**(2), 315-320.

O'Reilly, M. P. and B. M. New (1982) Settlements above tunnels in the United Kingdom-their magnitude and prediction. *Tunnelling* '82, 179-185.

Outzka, M. T., T. Yamazaki, T. Hashimoto, and T. Oumoto (1995) Ground movement around tunnelling. *Tsuchi-to-Kiso* (in Japanese), **43**(9), Series No. 452, 67-73.

Peck, R. B. (1969) Deep excavations and tunnelling in soft ground. *Proceedings of the 7th International Conference on Soil Mechanics and Foundation Engineering*, state-of-the-art Volume, pp. 225-290. Mexico City, Mexico.

Takemura, J., T. Kimura, and S. F. Wong (1990) Undrained stability of two-dimension unlined tunnel in soft soil. *Proceedings of JSCE (Geotechnical Eng.)*, **418/III-12**, 267-277.

Wu, G. A., F. S. Zhuang, and F. G. Wang (1997) Ground settlements due to shield tunnelling in soft clay. *7th Conference on Current Researches in Geotechnical Engineering in Taiwan*, pp. 1025-1032. Taipei, Taiwan, R.O.C.

軟土內隧道周圍土壤之變形

李崇正　吳秉儒　邱顯堯

國立中央大學土木工程學系

摘　要

軟土通隧引致周圍土壤變形，常導致鄰近結構受損。本文利用一系列離心模型試驗探討位於軟土之淺隧道，在破壞前後周圍土壤之變形。文中詳述試驗流程，並將地表及地下沈陷槽之試驗結果與現場觀測結果比較，兩者相當一致。深徑比在0.5-4間之淺隧道，破壞時之過荷重因子介於上下限解之間。從上限解得到之破壞型態與試驗觀測結果一致。本文分別建立地表及地下土層沈陷槽寬度參數及最大沈陷量與隧道深度及土壤漏失量之關係，可供進行鄰房保護設計時使用。